Spatio-temporal distribution of atomic and molecular excited species in LIBS: Potential implications on the determination of halogens

Luis Javier Fernández-Menéndez, Cristina Méndez-López, César Alvarez-Llamas, Cristina González-Gago, Jorge Pisonero, Nerea Bordel

PII: S0584-8547(20)30068-9

DOI: https://doi.org/10.1016/j.sab.2020.105848

Reference: SAB 105848

To appear in: *Spectrochimica Acta Part B: Atomic Spectroscopy*

Received date: 6 February 2020

Revised date: 26 March 2020

Accepted date: 28 March 2020

Please cite this article as: L.J. Fernández-Menéndez, C. Méndez-López, C. Alvarez-Llamas, et al., Spatio-temporal distribution of atomic and molecular excited species in LIBS: Potential implications on the determination of halogens, *Spectrochimica Acta Part B: Atomic Spectroscopy* (2020), https://doi.org/10.1016/j.sab.2020.105848

Spatio-temporal distribution of atomic and molecular excited species in LIBS: potential implications on the determination of halogens.

Luis Javier Fernández-Menéndez[1], Cristina Méndez-López[1], César Alvarez-Llamas[2], Cristina González-Gago[1], Jorge Pisonero[1] and Nerea Bordel[1*].

[1] *University of Oviedo, Department of Physics. Federico García Lorca 18, 33007, Oviedo, Spain.*
[2] *University of Málaga, Department of Analytical Chemistry, UMA LASERLAB, Jimenez Fraud 4, 29071 Málaga, Spain.*
** Corresponding author: bordel@uniovi.es*

Keywords: Laser Induced Breakdown Spectrocopy (LIBS), Spatio-temporal emission distributions, Molecular spectra, CaF emission bands, Halogen determination.

Abstract:

A LIBS experimental set-up is designed and evaluated to obtain the spatio-temporal distribution of atomic and molecular emission signals after the ablation of samples with different amounts of Ca and F. This analysis revealed separated temporal and spatial regions that maximized the atomic and molecular emission signals, respectively. Therefore, these distributions are investigated to elucidate the origin of the CaF molecular excited species, and to evaluate the development of an optimized method for the measurement of CaF molecular signals, which are related to the concentration of F in the sample.

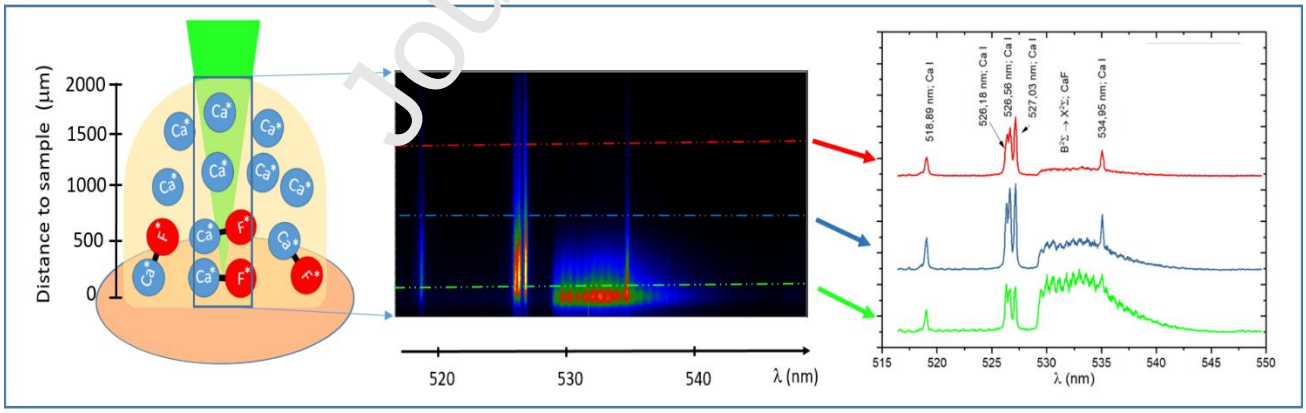

1. INTRODUCTION

Laser-Induced Breakdown Spectroscopy (LIBS) is an analytical technique based on the measurement of the emission spectrum from a laser induced plasma, which is created after the ablation of a sample by a short laser pulse with high irradiance (typically about 10^{10} W/cm^2) [1]–[4]. A spectroscopic analysis of the emitted light provides information about the chemical composition of the sample and gives insight regarding the physical parameters of the plasma (e.g. electronic/rotational temperatures and/or electron number densities). LIBS is known to provide fast analysis with high spatial resolution (e.g. micrometer lateral resolution and nanometer in-depth resolution [5]), as well as, to offer portability for in-situ analysis, and stand-off analysis potential [1]. Moreover, LIBS reaches adequate sensitivity for multi-elemental analysis in multiple fields of applications. Nevertheless, one major drawback of LIBS analysis is related to the determination of halogens with high sensitivity. These elements have relatively high excitation and ionization potentials (>10 eV) and most of their intense resonant emission lines are located in the vacuum ultraviolet spectral region, whose detection would require complex experimental set-ups. An approach for LIBS determination of halogen elements is the use of their near infrared (NIR) lines, which are relatively less intense, resulting in poor limits of detection (LOD) and quantification (LOQ). [6]

In recent years, many efforts have been made to improve halogen detection in LIBS. For instance, atomic emission of halogens was enhanced through the generation of the laser-induced plasma in a helium atmosphere [7], [8]. At these operating conditions, the electron density of the plasma plume was reduced, decreasing the background signal and improving the signal to background ratio of the NIR lines emitted by the halogens [9]. Alternatively, the use of molecular emission was successfully evaluated as an indirect way to determine the concentration of halogens in a sample [10]–[16]. Halides molecules are considered to be preferentially created by the combination of an alkaline earth and a halogen. For example, CaF molecular signal was proved to be very useful for the determination of F in Ca containing samples, offering improved sensitivity in comparison to the use of NIR F atomic emission lines [17], [18]. This method was also applied to non-containing Ca samples. In that case, Ca was externally introduced at the laser-induced plasma site making use of a nebulizer [19].

LIBS is based on the detection of emission signals in a dynamic plasma; therefore, the detector is synchronized with the ablation process to collect the plasma emission at the proper moment and with the adequate integration time for each application. The possibility of measuring the plasma with temporal resolution allows to understand how it evolves [20]. Additionally, spatially resolved studies can provide information about laser-induced plasma expansion and plume symmetry [21]–[23].

Furthermore, it can be employed to discriminate regions of maximum emission signal for different elements [24], to improve the limits of detection using atomic emissions [25] or to spatially select where molecular signal predominates over atomic/ionic signals [26]–[28]. In this line, studies with spatial and temporal resolution of CaF_2 ablation plumes carried out by Ouija *et al.* [29] showed that CaF species were responsible of harmonic generation of the fundamental radiation of a Q switched Nd-YAG directed parallel to the target surface, and Gaft *et al.* [14] carried out a preliminary study of CaF spatial distribution as a source for fluorine detection .

Spatio-temporal distributions of molecular signals were used to evaluate double pulse LIBS excitation processes [30], and to investigate the mechanisms of chemical species recombination within the plasma (e.g. presence of native species or associated to recombination with the surrounding gas species) [31]–[37]. Nevertheless, optimized detection methods based on the evaluation of spatio-temporal distributions of molecular excited species have not been yet investigated. Therefore, a combination of both spatial and temporal resolution to study molecular excited species in LIBS is here considered to optimize the detection of halides molecules within the plasma. Specifically, the spatio-temporal distribution of CaF molecular emission in several Ca and F containing samples is investigated, and this distribution is compared with that of atomic excited Ca species.

2. EXPERIMENTAL

2.1 LIBS set-up

A Q-Switched Nd:YAG laser (EKSPLA, NL301HT) operating at 1064 nm and 10 Hz repetition rate is used as excitation source. The laser pulse energy is fixed at 100 mJ using an attenuator (LOTIS-TII). The laser beam is focused on the sample surface using a 35 mm focal length objective (Thorlabs, LMH-5X-1064). Moreover, the sample is placed on a X-Y stage controlled by two stepper motors (PImiCos GmbH VT_80200-2SN and another one manufactured by the University of Oviedo). Plasma emission is collected by two plano-convex lenses (50.8 mm diameter), directly forming the plasma image on the spectrograph entrance slit plane. The first lens (Thorlabs, LA4904-UV) has a focal length of 150 mm and the second one (Thorlabs, LA4855-UV) has a focal length of 300 mm, resulting in a 2:1 magnification of the plasma plume. The detection system comprises a Czerny-Turner 500 mm focal length spectrograph (Andor Technology, Shamrock SR-500i-D1) coupled to an ICCD (Andor Technology, iStar DH734-25F-03), whose matrix has 1024x1024 pixels (with an effective pixel size of 19.5 x 19.5 μm). The spectrograph is equipped with a mirror and a grating of 1200 lines/mm. Figure 1 shows a schematic representation of the LIBS experimental set-up used in this work.

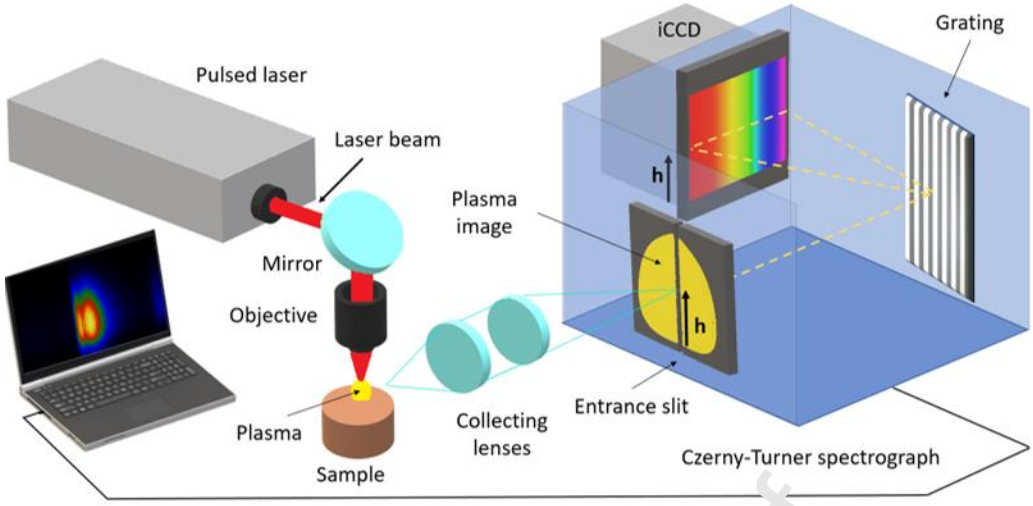

Figure 1. Schematic representation of the LIBS experimental set-up. This configuration allows the association of the collected spectrum in each horizontal row of the CCD with that emitted at a certain height (h) of the plasma.

Plasma image is formed at the entrance of the spectrograph in such a way that the vertical symmetry axis of the plasma meets the entrance slit (fixed at 100 µm width), as can be seen in Figure 1. Photons going through the slit at different heights are then diffracted, so that the spectrum measured at each row of the CCD can be related to the emission coming from a given height of the central region of the plasma.

The spatial resolving power provided by this experimental set-up was calibrated by means of a resolution test target 1951 USAF (Thorlabs, R3L3S1N). This test target was illuminated from the back and its image was formed at the spectrograph entrance with the slit completely open. Total light was collected using the mirror instead of a diffraction grating. The calculated spatial resolving power obtained from the image of the test target was 16 line pairs per mm thus providing an accuracy in distance determination of approximately 60 µm, since element 1 of group 4 from the USAF was the largest set with non-distinguishable horizontal lines. Likewise, the scale of the images formed in the CCD was calculated to be 9.6 $\pm$ 0.3 µm/pixel, i.e. approximately half the size of the pixel.

Considering the scale obtained by the USAF and identifying the row corresponding to the height on which the sample surface was placed, each row of the CCD was then associated with a plasma height.

2.2 Samples

Samples of CaF_2 (Alfa Aesar, [CaF_2] > 99.5 %), mixed samples of $CaCO_3$ (VWR Chemicals, [$CaCO_3$] > 98.5 %) and NaF (Alfa Aesar, [NaF] > 99.0 %), and mixed samples of CaF_2 and Cu (Alfa Aesar, [Cu] > 99.0 %), were used in this work. All of them were obtained from powder reference materials, which were properly mixed in an agate mortar keeping a molar ratio Ca:F (1:2). A set of sieves was used to estimate the particle sizes of the powders. For the CaF_2 sample, 80% of the mass of the sample is

related to particles with diameters between 63 and 250 μm. For the $CaCO_3$+NaF samples and the samples on Cu matrix, 80% of the mass consisted of particles with diameters between 63 and 125 μm.

Table 1 summarizes the percentage mass content of the samples. For each sample, an amount of 0.3 g of powder was homogeneously deposited on a double-sided tape fixed over a microscope slide. The excess powder was then removed, so that a small amount of material remains attached on the tape, with a thickness of one or two layers of powder (~200 μm). The slide was placed and horizontally levelled over the X-Y stage allowing ablating the mixtures.

Table 1. Mass concentration percentages of the different compounds in the analyzed samples.

Sample notation	% CaF_2	% $CaCO_3$	% NaF	% Cu
Sample 1	100	----	----	----
Sample 2	----	54.5	45.5	----
Sample 3	1	----	----	99

2.3 Acquisition conditions

Each sample was analyzed in raster mode (spot diameter at 400 μm, laser frequency at 10 Hz and sample translation at a speed of 4 mm/s) resulting in single shot ablation at each sample site. Spectra were collected at different delay times (t_d) from 0.4 μs to 135 μs. The spectral window obtained using the described experimental set-up covers a region of about 35 nm per exposition. Initially, spectra were collected every 0.2 μs since a fast plasma evolution takes place at short delay times after the laser shot; however, this integration time was progressively increased at longer delay times. Table 2 lists the experimental acquisition conditions used at the different delay times. Moreover, a correlation factor was calculated to compare spectra collected at delays (i.e. different acquisition conditions). This factor was achieved by comparing the intensities obtained for the same delay time when measured under two different acquisition conditions. Gain of the ICCD was fixed for all the measurements at a value that avoid exceeding the linear range of the CCD (40000 counts). Experimental data showed throughout this work were obtained from repeating the experiments in triplicate.

Table 2. Gate width, delay time step and number of software accumulations are given for each delay range. Note that one software accumulation compromises the acquisition of 12 successive plasma generated spectra, accumulated on the CCD chip.

Delay time range (μs)	Time step (μs)	Gate width (μs)	Accumulations on software		
			Sample 1	Sample 2	Sample 3
0.4 – 3	0.2	0.2	4	12	6
3 – 5	1	0.2	4	12	6
7	--	0.2	4	12	6
10 - 15	5	0.2	4	12	6
15 – 40	5	2	4	12	6
40 – 60	5	5	4	12	6
60 – 135	15	5	8	12	12

3. RESULTS AND DISCUSSION

3.1 Spatio-temporal distribution of Ca-related atomic emission and CaF-related molecular emission.

Laser induced plasma was initially investigated in a high purity CaF_2 sample (Sample 1). Emissions from CaF molecule were taken as a reference to study the distribution of molecular emission within the plasma plume. Specifically, the sequence $\Delta v=0$ of the $B^2\Sigma \rightarrow X^2\Sigma$ emission system was considered as it does not present appreciable spectral interference with other molecular bands for the analyzed samples [38]. Diffracting grating was then centred at 533.00 nm, covering the region between 516.42-549.60 nm, where it was possible to record the $B^2\Sigma \rightarrow X^2\Sigma$ system of CaF. Figure 2a shows the spectral CCD image of the plasma at three different delay times in the selected spectral region (emission signals were normalized at each represented delay). For early delay times (e.g. 1 μs delay time), LIBS spectrum was dominated by atomic emission from Ca I lines (molecular signal is negligible). Moreover, it is observed that the highest atomic emission signals occurred at a distance of 500 μm to the sample surface. At a delay of 10 μs, continuous background was significantly reduced, and atomic emission lines were spectrally narrower but with higher spatial extension in the vertical direction. Furthermore, molecular emission was enhanced and spatially separated from atomic emission (e.g. highest molecular emission signals were observed at shorter distances to the sample surface (about 120 μm)). After 60 μs, only molecular emission was detected with a broad spatial extension in the vertical direction (e.g. highest molecular emission signals were then observed

at distances ≥500 μm to the surface). It is therefore noticed that molecular emissions took longer times to expand and to completely attenuate their emission signals.

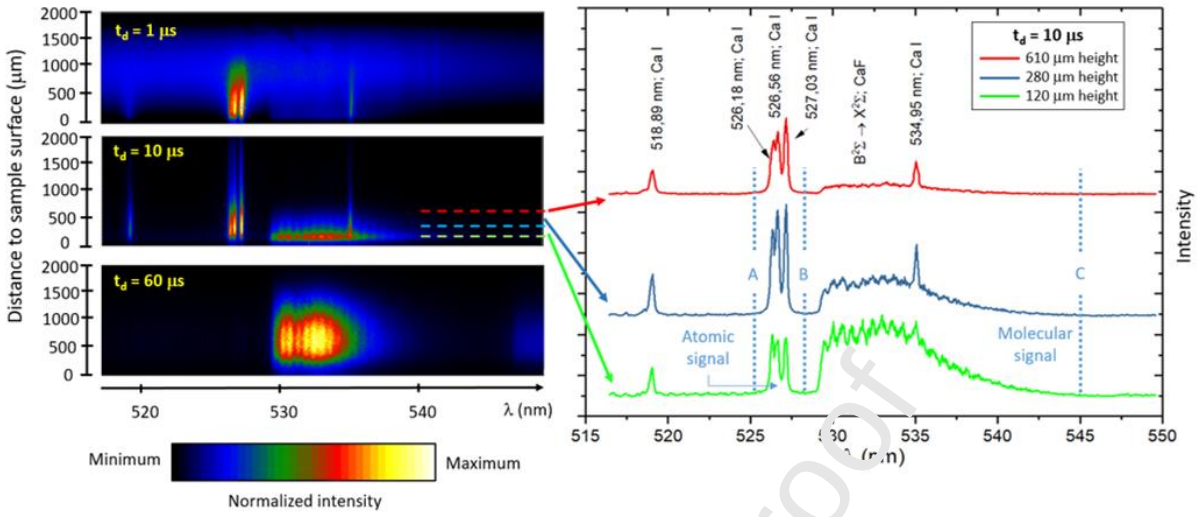

(a) (b)

Figure 2. (a) Spectral CCD images collected for the laser induced plasma in a CaF sample, at three different delay times (t_d). (b) Spectra collected in 3 different rows of the CCD (marked by dashed lines in a) at a 10 μs delay time. The integration spectral regions used to quantify both the atomic signal (A-B) and the molecular signal (B-C) are displayed.

Figure 2b shows three spectra measured at different distances to the sample surface (120, 280 and 610 μm, respectively) at a delay time of 10 μs (the corresponding acquisition rows are marked in Figure 2a by means of the dashed colour lines). Higher molecular to atomic emission ratio is clearly observed at low distances to the sample surface.

To obtain spatial emission distributions along the central axis of the plasma at a given delay, net integrated intensities (with background subtraction) related to atomic and molecular emission signals in each spectrum were calculated. Integration range for atomic emission was considered between 525.21 and 529.01 nm (A-B in Figure 2b), while the integration range for molecular emission was evaluated between 529.01 and 542.50 nm (B-C in Figure 2b). It should be remarked that emission signal from Ca I at 534.95 nm, which interferes with $B^2\Sigma \rightarrow X^2\Sigma$ system of CaF, was removed from the molecular emission contribution. These spatial distributions, calculated for all the considered delay times (from 0.4 to 135 μs), provided a detailed spatio-temporal evolution of the atomic and molecular contributions, which are plotted in Figure 3(a, b), respectively. Figure 3a shows the emission distribution of Ca atomic excited species, since early delay times until its extinction at approximately 60 μs. The emission was expanded during the first 5 μs after the ablation process, followed by a subsequent contraction. This behavior may be due to changes in plasma excitation, as well as to the downward movement of the emitting species within the plume. In this respect, Chen *et al.* [22] suggested that a low pressure zone is generated in the lower part of the plasma after its fast

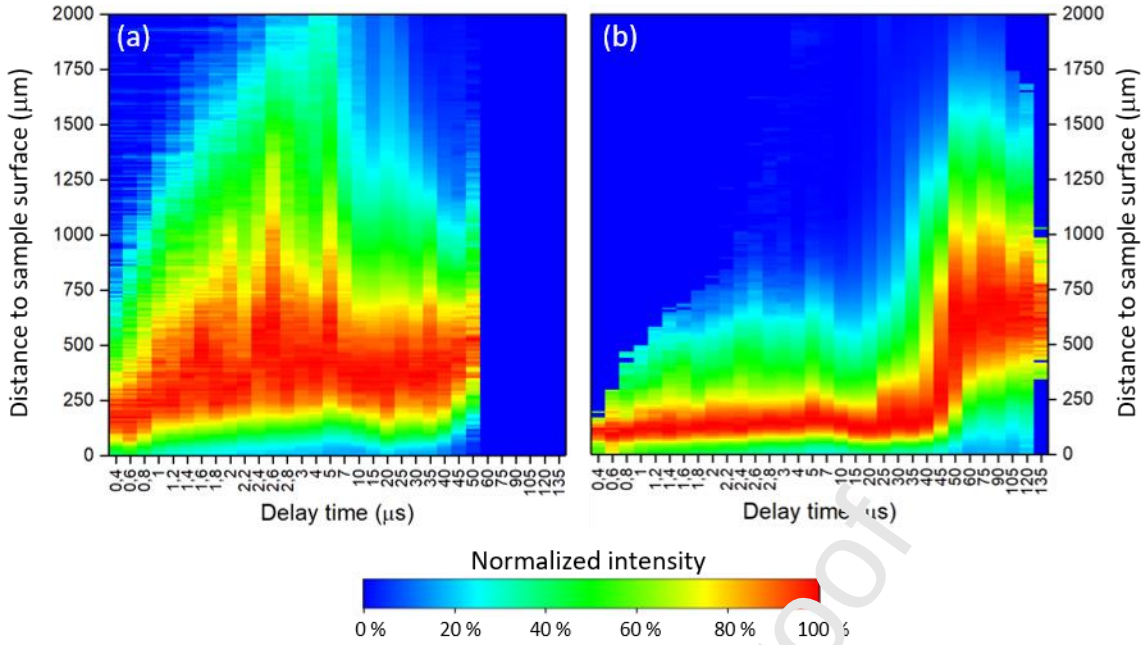

Figure 3. Distribution of the emission signal along the central axis of the plasma induced in the CaF_2 sample for: a) Atomic integrated contribution (on the left); b) Molecular integrated contribution (on the right). Emission signals were normalized to the respective maximum intensity at each delay time.

propagation. Moreover, other authors [39] also suggested that at the edge of the main shock wave, a secondary shock wave is generated propagating back into the plasma, making all the plasma emitters move downwards. Figure 3b shows that CaF molecular emission remained closer to the sample surface; however, at delay time larger than 45 μs (e.g. delays at which atomic emission signal starts to be negligible), the molecular signal was expanded away from the surface. Specifically, the highest values of CaF molecular emission intensity were observed at short distance to the sample surface (< 250 μm) during the first 45 μs, moving afterwards to further distances between 500 and 750 μm.

For a better understanding of the spatio-temporal dynamics, Figure 4a shows the distance-to-surface position of the maximum atomic and molecular emission signal recorded at each delay time. The total intensity acquired through the whole CCD is also plotted for both emissions as a function of the delay time (Figure 4b). Attending to the position of the maxima, four temporal regions were differentiated in Figure 4a: (1) until 5 μs the distance-to-surface of both atomic and molecular maxima emissions increased; (2) between 5 and 30 μs, where distance-to-surface for both highest emission signals experienced a small contraction and stabilized around 375 μm (atomic emission) and 150 μm (molecular emission), respectively; (3) between 30 and 60 μs, where distance-to-surface for both maxima moved up again; (4) after 60 μs, where only molecular signal persisted and its maxima position remained stable. Regarding the total integrated contribution (Figure 4b), it is observed that atomic emission signal showed a monotonic decay, while molecular emission signal achieved a maximum at a delay time of 7 μs, which is a relatively short delay compared to those employed for molecular detection in other works [17]–[19], [40], [41] .

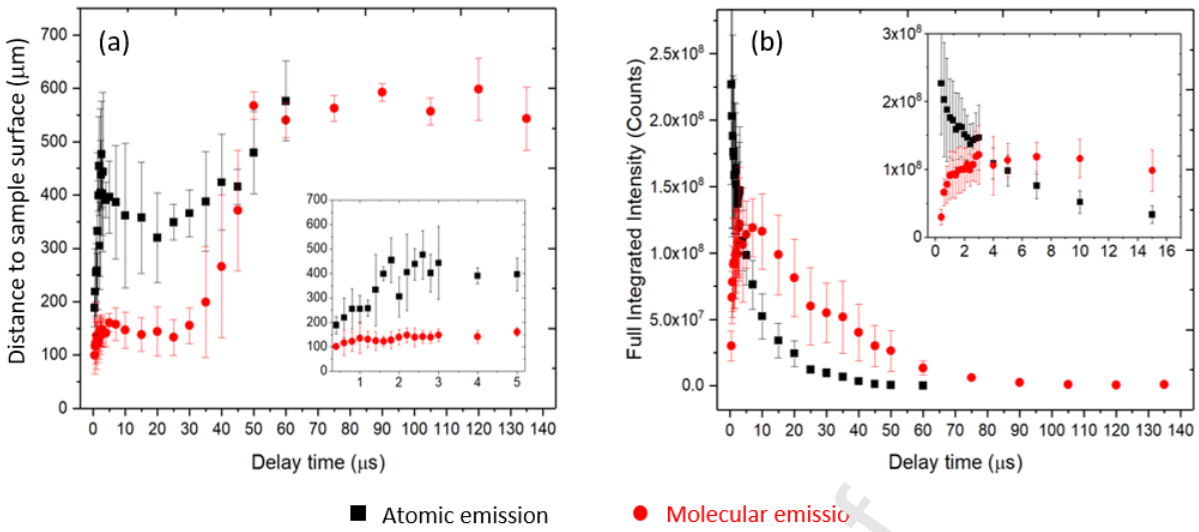

Figure 4. (a) Distance-to-surface of the maximum emission for atomic (black) and molecular (red) signals measured in a pure CaF_2 sample, in terms of the delay time. (b) Evolution of the full integrated intensity (accumulating all rows of the CCD) as a function of delay time (graphic insets show early delay results).

An explanation for the upward expansion of CaF radiation after 45 μs relies on the fact that Ca-F recombination processes begin to be predominant throughout the height of the plasma. It is at this moment when molecular radiation maxima tend to occupy the position previously occupied by atomic emission maxima (Figure 4a). Alternatively, molecular emission in the proximities of the sample surface at short delay times (< 45μs) could be due to the emission of no dissociated native Ca-F bonds. Further insights to elucidate the potential origin of these excited molecules requires the determination of the spatio-temporal distribution of CaF molecular emission in matrices that do not contain native CaF bonds.

3.2 Spatio-temporal distribution of CaF molecular emission in samples with non-native CaF bonds.

Figure 5(a,b) shows the spatio-temporal distribution of integrated Ca (525.21 – 529.01 nm) and CaF (529.01 – 542.50 nm) emission signals, after ablation of a sample without native CaF bonds. In this case, the sample consisted of a $CaCO_3$+NaF mixture (Sample 2). It is observed that maxima displacements of emissions (atomic and molecular) with respect to the sample surface was achieved at longer delay times and reached higher values, when compared to the spatio-temporal distributions measured after the ablation of the CaF_2 sample. Figure 6(a,b) shows the distance to surface of the maxima as well as the total intensity recorded for the atomic and molecular integrated contributions, respectively, as a function of the delay time. It is noticed that the spatial gap between the maximun signal for atomic and molecular contributions can be as large as 400 μm, which is greater that the gap obtained when ablating the CaF_2 sample (up to 225 μm). Ca atomic emission signal also showed a fast decay, while CaF molecular emission signal showed a first maximum at a delay time of 3 μs and remains stable until 50 μs. In addition, the comparison of Figure 4b and Figure

6b reveals that the ratio of molecular to atomic emission signal was smaller for Sample 2. It is considered that a decrease of the CaF molecular signal might be due to the higher presence of O in Sample 2 (e.g. a certain proportion of Ca available for the formation of CaF might be displaced to form CaO [27], [42]). These results shows that not only the CaF emission at long delays is due to recombination processes of Ca and F atoms but also the intense CaF molecular emission observed at early delays close to the sample surface can be attributed to these processes.

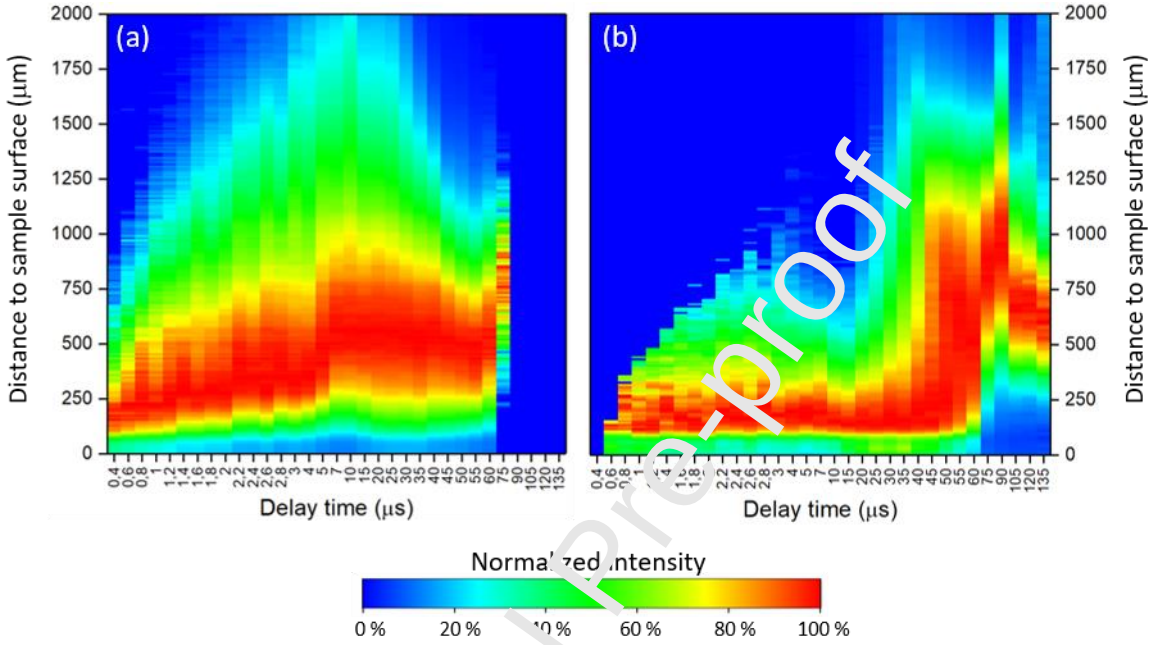

Figure 5. Distribution of the emission signals along the central axis of the plasma for: a) Integrated Ca atomic signals (on the left), b) integrated CaF molecular emissions (on the right); obtained for the sample 2 ($CaCO_3$+NaF). The signals were normalized to the respective maximum intensity at each delay time.

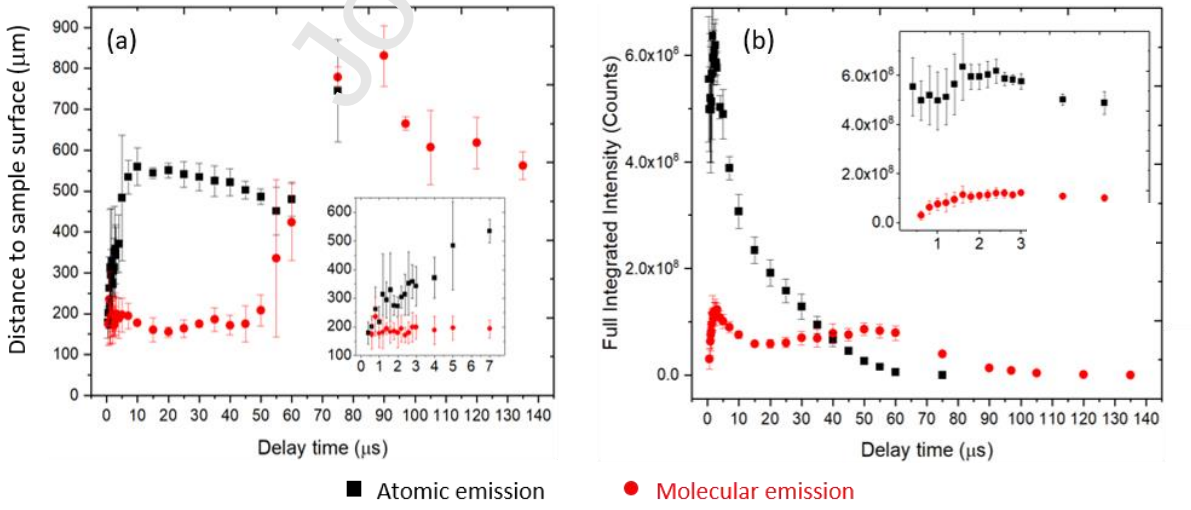

Figure 6. (a) Distance-to-surface of the maximum emission for atomic (black) and molecular (red) signals measured a mixture of $CaCO_3$ + NaF (Sample 2), in terms of the delay time. (b) Evolution of the full integrated intensity (accumulating all rows of the CCD) as a function of delay time (graphic insets show early delay results).

3.3 Determination of the concentration of low amounts of CaF selecting the proper spatio-temporal conditions.

So far, the distribution of Ca and CaF excited species was evaluated in samples where Ca and F were major elements (samples 1 and 2). However, these excited species could be affected in the laser-induced plasma by the presence of other elements in higher concentrations. Therefore, spatio-temporal studies were carried out using samples with lower concentration of CaF_2 (50, 25, 14, 4, 2, 1 and 0.5 wt. %) in a Cu matrix. LIBS analysis were performed using the procedure described in previous sections, centring the diffraction grating at 540 nm. Analogous spatio-temporal distributions of the emission signals (both atomic and molecular) to those obtained for Samples 1 and 2 were measured in all the samples. As an example, Figure 7 shows the spatio-temporal distribution of the emission signals for the sample with a concentration of 1 wt. % CaF_2 (labelled as Sample 3). Emission distributions of the other samples with different concentrations of CaF_2 are plotted in Figure 1S (see supplementary information).

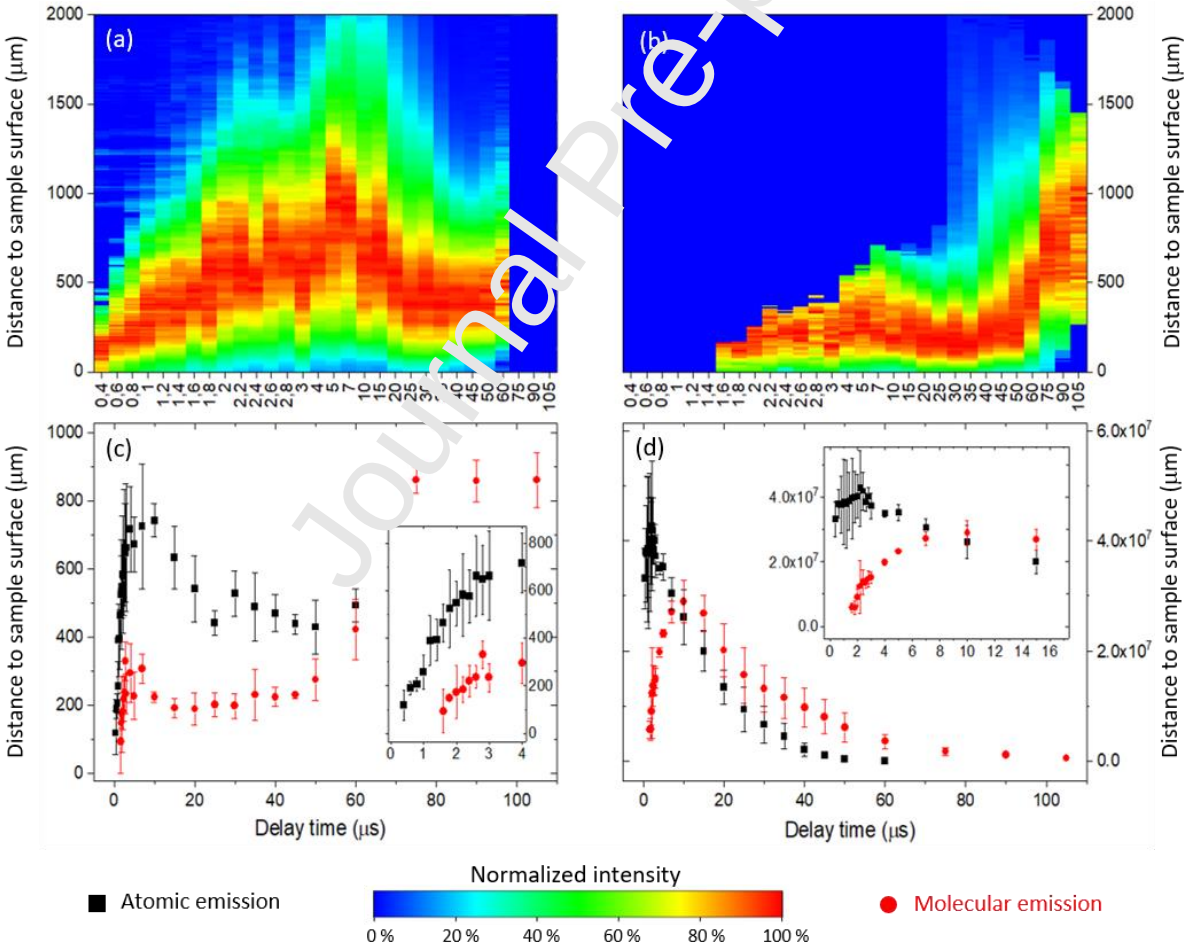

Figure 7. Distribution of the emission signals along the central axis of the plasma for: a) Ca atoms (on the left), b) CaF molecules (on the right) using the sample 3 (Cu+CaF_2). The signals were normalized to the respective maximum intensity at each delay time. The origin of height was fixed at the sample surface. (c) Positions of maximum atomic (black) and

molecular (red) signals vs. delay time. (d) Evolution of the full integrated intensity (accumulating all rows of the CCD) as a function of delay time (graphic insets (in c and d) show early delay results).

The spatial gap observed at short delay times (between 5 and 60 μs) between the highest atomic and molecular emission signals might be employed to acquire the molecular signal at the distances to sample surface, where the contribution of atomic signals is significantly reduced. By comparing Figure 7 with the results obtained in sections 3.1 and 3.2, it can be seen that the emission distributions in all cases meet two conditions: there is a spatial separation between atomic and molecular emissions removing possible spectral interference among them, and the maximum molecular intensity appears at the same time as this spatial splitting is present. These properties can then be used to improve the detection of the molecular signal. Thus, different spatial regions were evaluated to measure CaF molecular emission in Sample 3. Figure 8 shows the spectra obtained in 4 different spatial regions (e.g. 0-240, 240-480, 480-720 and 720-960 μm respectively). Each of these regions corresponds to 25 rows of the CCD. The corresponding 25 spectra were added up into a single spectrum per region. It is observed that spectrum in region A (0-240 μm) shows a low contribution of atomic lines. This contribution increases when considering longer distances to the sample surface. Nevertheless, spectrum in region B (240-480 μm) showed the highest molecular emission with a still-reduced atomic contribution. Spectra in regions C and D showed significantly higher atomic emission contribution while decreasing molecular signal. These results indicate that a proper spatial region to measure the CaF emission signal is that from 0 to 480 μm, while simultaneously the adequate region for the atomic emission is that from 480 to 960 μm.

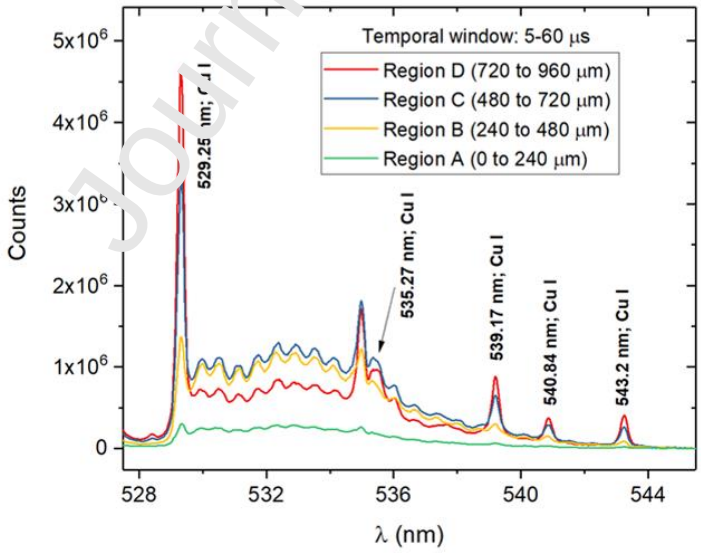

Figure 8. Spectra accumulated in 4 spatial regions (e.g. different distances to the sample surface) using a delay time of 5 μs and a gate of 55 μs.

Figure 9 compares the spectrum obtained at the optimized spatio-temporal conditions with that obtained using typical molecular acquisition conditions (temporal window between 60 and 160 µs and integrating the whole spatial plasma region), employed in previous works [17]–[19].

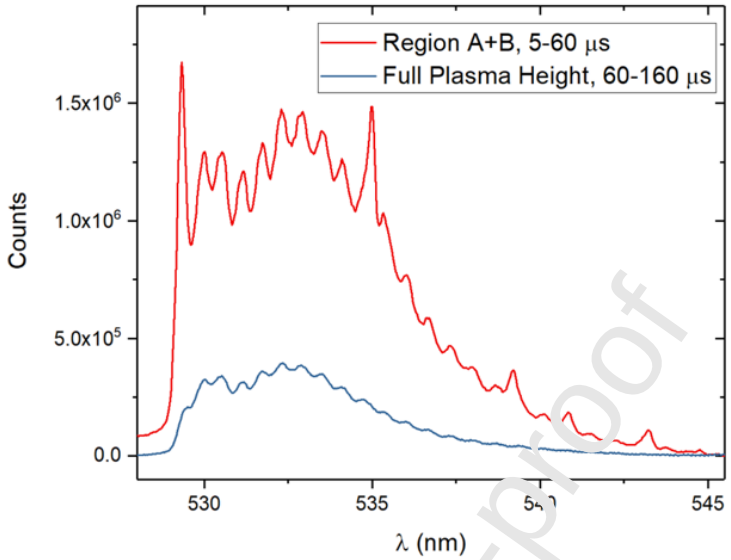

Figure 9. Molecular spectra obtained from the Cu matrix with 1 wt. % CaF_2. (a) Spectra accumulated at distance to sample surface between 0 and 480 µm using a temporal window between 5 and 60 µs, and molecular spectra accumulated at standard conditions (full plasma height in the 60-180 µs temporal window).

The optimized spatio-temporal conditions provided an improved molecular signal (more than 4 times higher). In order to evaluate the possibilities of this methodology for the determination of halogens, the calibration curve for F concentration was evaluated. Figure 10 shows the calibration curves obtained for samples that consisted of a Cu matrix with different concentrations of CaF_2 (4, 2, 1, 0.2 and 0.1 wt. %) that correspond to several concentrations of F (1.95, 0.97, 0.49, 0.10 and 0.05 wt. %), respectively. All these samples were analyzed under optimal conditions (temporal window 5-60 µs and spatial region between 0 and 480 µm). A linear response was observed when plotting the net CaF molecular emission signals versus the concentrations of F in the samples. In addition, for comparative purposes, the samples were also analyzed at typical molecular acquisition conditions (integrating the signal from the whole plasma height in a temporal window 60 – 160 µs) and the calibration curve is included in Figure 10. It is observed that the optimized acquisition conditions provided a calibration curve with a slope more than 4 times higher, showing the significant enhancement on the sensitivity of these measurements.

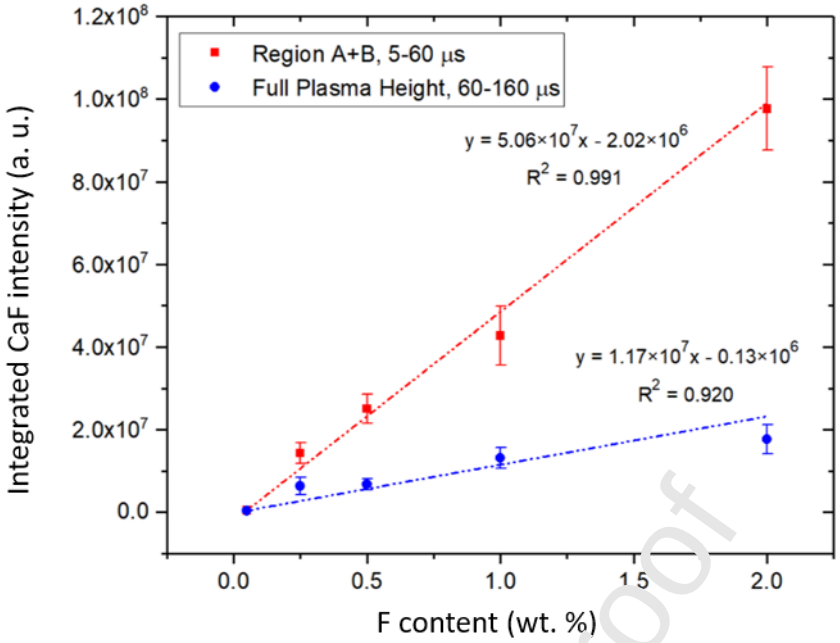

Figure 10. Calibration curves for the concentration of F. In red, the calibration curve obtained by integrating the CaF molecular signal at the optimized spatio-temporal conditions (e.g. spectra accumulated at distance to sample surface between 0 and 480 μm using a temporal window between 5 and 60 μs). In blue, the calibration curve obtained by integrating the CaF molecular signal at the typical molecular acquisition conditions (spectra accumulated in the full plasma height using a temporal window between 60 and 160 μs).

4. Conclusions

The spatio-temporal distribution of atomic and molecular emission in a LIBS plasma, obtained from samples with high amounts of Ca and F (e.g. CaF_2 matrix with native Ca-F bonds, and $CaCO_3$+NaF matrix without native Ca-F bonds), showed similar behaviour, indicating that, under the analized experimental conditions, CaF excited molecular species were mainly formed by recombination processes of these species.

The spatial distribution of atomic and molecular excited species showed a splitting at delay times smaller than 60 μs. In particular, molecular emission was predominant at closer distances to the sample surface (between 0 and 480 μm), while atomic emission was enhanced at longer distances to the sample surface. At longer delay times (>60 μs), atomic emission signals became negligible while molecular signals persisted; although the maxima emission was displaced to longer distances to the sample surface.

This spatio-temporal splitting of atomic and molecular signals was used to optimize the acquisition conditions that maximise the CaF molecular emission while keeping at low levels the atomic emission. Using these conditions, a linear calibration curve was successfully achieved for low concentrations of CaF_2 in a Cu matrix, improving the sensitivity for F detection by more than 4 times, in comparison to that obtained using typical molecular acquisition conditions.

We believe that this methodology has a great potential for the simultaneous quantification of halogens (via detection of molecular signals from halide compounds) and other species (via detection of atomic and ionic signals).

Acknowledgments

The authors gratefully acknowledge the financial support of the Spanish Government through the project MINECO 17-CTQ2016-77887-C2-1R and the pre-doctoral grant MINECO BES-2017-080768. Financial support from the Government of the Principality of Asturias (Fondos Feder) through the project GRUPIN IDI-2018-000186 is also recognized.

Conflicts of Interest

The authors declare no conflict of interest

References

[1] D. A. Cremers and L. J. Radziemski, *Handbook of Laser-induced Breakdown Spectroscopy*. Chichester, UK: John Wiley & Sons, Ltd, 2006.

[2] R. E. Russo, X. L. Mao, J. H. Yoo, and J. J. Gonzalez, "Laser Ablation", *Laser-Induced Break. Spectrosc.*, pp. 49–82, Jan. 2007.

[3] D. W. Hahn and N. Omenetto, "Laser-induced breakdown spectroscopy (LIBS), part I: Review of basic diagnostics and plasma–particle interactions: Still-challenging issues within the analytical plasma community", *Appl. Spectrosc.*, vol. 64, no. 12, 2010.

[4] D. W. Hahn and N. Omenetto, "Laser-induced breakdown spectroscopy (LIBS), part II: Review of instrumental and methodological approaches to material analysis and applications to different fields", *Appl. Spectrosc.*, vol. 66, no. 4, pp. 347–419, Apr. 2012.

[5] L. M. Cabalín, A. González, V. Lazic, and J. Laserna, "Deep ablation and depth profiling by laser-induced breakdown spectroscopy (LIBS) employing multi-pulse laser excitation: Application to galvanized steel", *Appl. Spectrosc.*, vol. 65, no. 7, pp. 797–805, Jul. 2011.

[6] D. E. Anderson *et al.*, "Characterization of LIBS emission lines for the identification of chlorides, carbonates, and sulfates in salt/basalt mixtures for the application to MSL ChemCam data", *J. Geophys. Res. Planets*, vol. 122, no. 4, pp. 744–770, Apr. 2017.

[7] M. Tran, Q. Sun, B. W. Smith, and J. D. Winefordner, "Determination of F, Cl, and Br in solid organic compounds by laser-induced plasma spectroscopy", *Appl. Spectrosc.*, vol. 55, no. 6,

pp. 739–744, Jun. 2001.

[8] D. A. Cremers and L. J. Radziemski, "Detection of Chlorine and Fluorine in Air by Laser-Induced Breakdown Spectrometry", *Anal. Chem.*, vol. 55, no. 8, pp. 1252–1256, Jul. 1983.

[9] L. St-Onge, E. Kwong, M. Sabsabi, and E. B. Vadas, "Quantitative analysis of pharmaceutical products by laser-induced breakdown spectroscopy", *Spectrochim. Acta - Part B At. Spectrosc.*, vol. 57, no. 7, pp. 1131–1140, Jul. 2002.

[10] S. Millar, C. Gottlieb, T. Günther, N. Sankat, G. Wilsch, and S. Kruschwitz, "Chlorine determination in cement-bound materials with Laser-induced Breakdown Spectroscopy (LIBS) – A review and validation", *Spectrochim. Acta - Part B At. Spectrosc.*, vol. 147, pp. 1–8, Sep. 2018.

[11] T. Dietz, J. Klose, P. Kohns, and G. Ankerhold, "Quantitative determination of chlorides by molecular LIBS", *Spectrochim. Acta - Part B At. Spectrosc.*, vol. 152, pp. 59–67, Feb. 2019.

[12] N. Omenetto, W. B. Jones, B. W. Smith, T. Guenther, E. Ewusi-Annan, and U. of Florida, "Feasibility of atomic and molecular laser induced breakdown spectroscopy (LIBS) to in-situ determination of chlorine in concrete : final report.", Oct. 2016.

[13] O. Forni *et al.*, "First detection of fluorine on Mars: Implications for Gale Crater's geochemistry", *Geophys. Res. Lett.*, vol. 42, no. 4, pp. 1020–1028, Feb. 2015.

[14] M. Gaft, L. Nagli, N. Eliezer, Y. Groisman, and O. Forni, "Elemental analysis of halogens using molecular emission by laser-induced breakdown spectroscopy in air", *Spectrochim. Acta - Part B At. Spectrosc.*, vol. 98, no. June, pp. 39–47, 2014.

[15] D. S. Vogt, K. Rammelkamp, S. Schröder, and H. W. Hübers, "Molecular emission in laser-induced breakdown spectroscopy: An investigation of its suitability for chlorine quantification on Mars", *Icarus*, vol. 302, pp. 470–482, Mar. 2018.

[16] D. S. Vogt, S. Schröder, K. Rammelkamp, P. B. Hansen, S. Kubitza, and H.-W. Hübers, "CaCl and CaF emission in LIBS under simulated Martian conditions", *Icarus*, vol. 335, p. 113393, Jan. 2020.

[17] C. Álvarez, J. Pisonero, and N. Bordel, "Quantification of fluorite mass-content in powdered ores using a Laser-Induced Breakdown Spectroscopy method based on the detection of minor elements and CaF molecular bands", *Spectrochim. Acta - Part B At. Spectrosc.*, vol. 100, pp. 123–128, Oct. 2014.

[18] C. Alvarez-Llamas, J. Pisonero, and N. Bordel, "Quantification of fluorine traces in solid samples using CaF molecular emission bands in atmospheric air LIBS", *Spectrochim. Acta - Part B At. Spectrosc.*, vol. 123, pp. 157–162, Sep. 2016.

[19] C. Alvarez-Llamas, J. Pisonero, and N. Bordel, "A novel approach for quantitative LIBS fluorine analysis using CaF emission in calcium-free samples", *J. Anal. At. Spectrom.*, vol. 32, no. 1, pp. 162–166, 2017.

[20] A. De Giacomo and J. Hermann, "Laser-induced plasma emission: From atomic to molecular spectra", *J. Phys. D. Appl. Phys.*, vol. 50, no. 18, 2017.

[21] P. Yeates and E. T. Kennedy, "Spectroscopic, imaging, and probe diagnostics of laser plasma plumes expanding between confining surfaces", *J. Appl. Phys.*, vol. 108, no. 9, 2010.

[22] A. Chen, Y. Jiang, H. Liu, M. Jin, and D. Ding, "Plume splitting and rebounding in a high-intensity CO_2 laser induced air plasma", *Phys. Plasmas*, vol. 19, no. 7, 2012.

[23] M. Momcilovic *et al.*, "Optical emission studies of copper plasma induced using infrared transversely excited atmospheric (IR TEA) carbon dioxide laser pulses", *Appl. Spectrosc.*, vol. 69, no. 4, pp. 419–429, 2015.

[24] C. Li, D. Zhao, X. Wu, and H. Ding, "Spatial resolution measurements of C, Si and Mo using LIBS for diagnostics of plasma facing materials in a fusion device", *Plasma Sci. Technol.*, vol. 17, no. 8, pp. 638–643, Aug. 2015.

[25] D. Sun, Y. Ma, Y. Wang, M. Su, Q. Lu, and C. Dong, "Determination of the limits of detection for aluminum-based alloys by spatially resolved single- and double-pulse laser-induced breakdown spectroscopy", *Anal. Methods*, vol. 10, no. 22, pp. 2595–2603, 2018.

[26] A. A. Bol'Shakov, X. Mao, J. J. González, and R. E. Russo, "Laser ablation molecular isotopic spectrometry (LAMIS): Current state of the art", *J. Anal. At. Spectrom.*, vol. 31, no. 1, pp. 119–134, Dec. 2016.

[27] A. A. Bol'Shakov, X. Mao, and R. E. Russo, "Spectral emission enhancement by an electric pulse for LIBS and LAMIS", *J. Anal. At. Spectrom.*, vol. 32, no. 3, pp. 657–670, 2017.

[28] C. Koral, A. De Giacomo, X. Mao, V. Zorba, and R. E. Russo, "Nanoparticle Enhanced Laser Induced Breakdown Spectroscopy for Improving the Detection of Molecular Bands", *Spectrochim. Acta - Part B At. Spectrosc.*, vol. 125, pp. 11–17, 2016.

[29] M. Oujja, R. De Nalda, M. López-Arias, R. Torres, J. P. Marangos, and M. Castillejo, "CaF_2

ablation plumes as a source of CaF molecules for harmonic generation", *Phys. Rev. A - At. Mol. Opt. Phys.*, vol. 81, no. 4, p. 043841, Apr. 2010.

[30] A. De Giacomo, M. Dell'Aglio, D. Bruno, R. Gaudiuso, and O. De Pascale, "Experimental and theoretical comparison of single-pulse and double-pulse laser induced breakdown spectroscopy on metallic samples", *Spectrochim. Acta - Part B At. Spectrosc.*, vol. 63, no. 7, pp. 805–816, 2008.

[31] S. Acquaviva and M. L. De Giorgi, "Temporal and spatial analysis of plasmas during graphite laser ablation in low-pressure N 2", *Appl. Surf. Sci.*, vol. 197–198, pp. 21–26, 2002.

[32] S. S. Harilal, B. E. Brumfield, B. D. Cannon, and M. C. Phillips, "Shock Wave Mediated Plume Chemistry for Molecular Formation in Laser Ablation Plasmas", *Anal. Chem.*, vol. 88, no. 4, pp. 2296–2302, Feb. 2016.

[33] H. Hou, B. Yang, X. Mao, V. Zorba, P. Ran, and R. E. Russo, "Characteristics of plasma plume in ultrafast laser ablation with a weakly ionized air channel", *Opt. Express*, vol. 26, no. 10, p. 13425, 2018.

[34] S. A. Irimiciuc, B. C. Hodoroaba, G. Bulai, S. Gurlui, and V. Craciun, "Multiple structure formation and molecule dynamics in transient plasmas generated by laser ablation of graphite", *Spectrochim. Acta - Part B At. Spectrosc.*, vol. 165, no. 409, 2020.

[35] E. J. Kautz *et al.*, "Time-resolved imaging of atoms and molecules in laser-produced uranium plasmas", *J. Anal. At. Spectrom.*, vol. 34, no. 11, pp. 2236–2243, 2019.

[36] P. Ran, H. Hou, and S. N. Luo, "Molecule formation induced by non-uniform plume-air interactions in laser induced plasma", *J. Anal. At. Spectrom.*, vol. 32, no. 11, pp. 2254–2262, 2017.

[37] R. Glaus, J. Riedel, and I. Gornushkin, "Insight into the Formation of Molecular Species in Laser-Induced Plasma of Isotopically Labeled Organic Samples", *Anal. Chem.*, vol. 87, no. 19, pp. 10131–10137, 2015.

[38] R. W. B. Pearse and A. G. Gaydon, *The identification of molecular spectra*. Chapman & Hall, 1976.

[39] N. Arnold, J. Gruber, and J. Heitz, "Spherical expansion of the vapor plume into ambient gas: An analytical model", *Appl. Phys. A Mater. Sci. Process.*, vol. 69, no. 7, pp. S87–S93, Dec. 1999.

[40] X. Mao, A. A. Bol'Shakov, D. L. Perry, O. Sorkhabi, and R. E. Russo, "Laser Ablation Molecular

Isotopic Spectrometry: Parameter influence on boron isotope measurements", *Spectrochim. Acta - Part B At. Spectrosc.*, vol. 66, no. 8, pp. 604–609, Aug. 2011.

[41] V. Lazic, A. Palucci, S. Jovicevic, C. Poggi, and E. Buono, "Analysis of explosive and other organic residues by laser induced breakdown spectroscopy", *Spectrochim. Acta - Part B At. Spectrosc.*, vol. 64, no. 10, pp. 1028–1039, Oct. 2009.

[42] T. Dietz, P. Kohns, and G. Ankerhold, "Diagnostics and simulations of molecular formation in laser-induced plasmas", *Spectrochim. Acta - Part B At. Spectrosc.*, vol. 148, pp. 51–59, Oct. 2018.

Author Statement

Author Contributions:

Conceptualization: L.J.F.-M., C.M.-L., C.A.-L., J.P. and N.B

Funding Acquisition: J.P. and N.B.

Investigation: L.J.F.-M., C.M.-L., C.A.-L., and N.B.

Writing—Original Draft Preparation: L.J.F.-M.

Writing—Review & Editing: L.J.F.-M, C. G.-G, J.P and N.B.

Supervision: C. G.-G; J.P and N.B.

Declaration of interests

■ The authors declare that they have no known competing financial interests or person al relationships that could have appeared to influence the work reported in this paper.

☐The authors declare the following financial interests/personal relationships which may be considered as potential competing interests:

Highlights

- Novel LIBS method for fluorine detection.
- Spatial splitting between atomic and molecular emission in the plasma.
- Analytical sensitivity improvement for F determination.

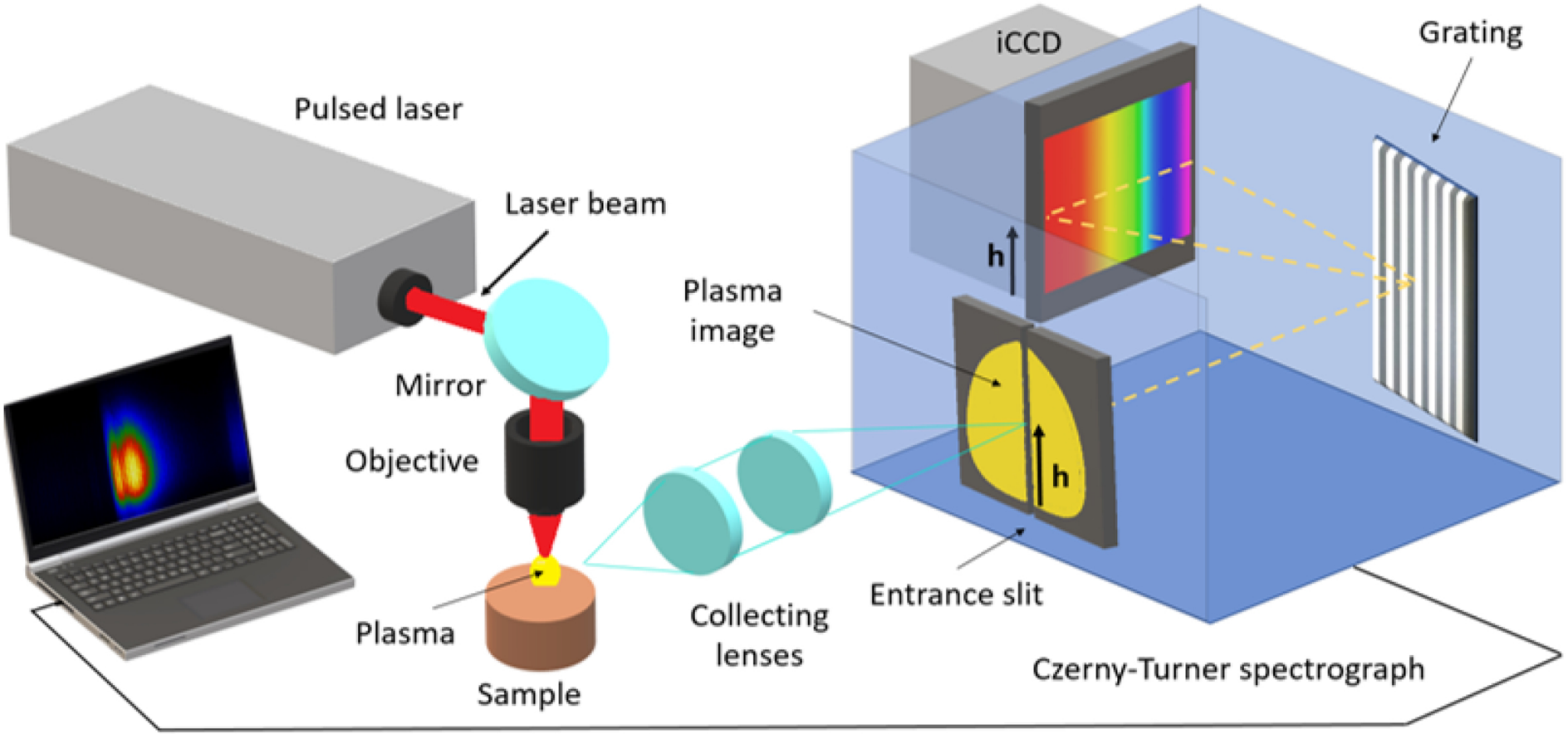
iCCD
Grating
Pulsed laser
Laser beam
h
Plasma
image
Mirror
Objective
h
Plasma
Collecting
lenses
Entrance slit
Sample
Czerny-Turner spectrograph

Figure 1

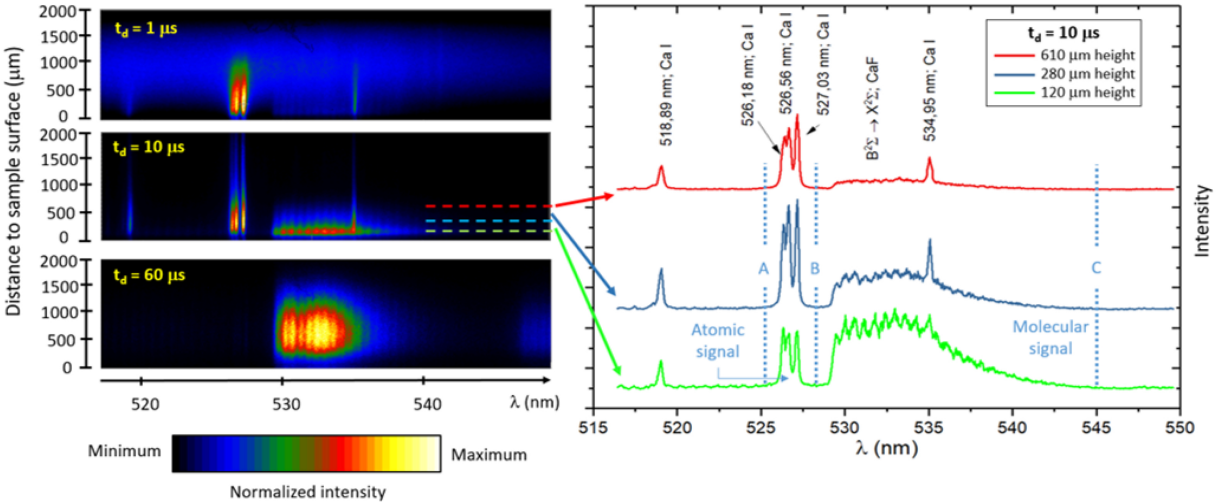
Distance to sample surface (µm)
2000
1500
1000
500
0
t_d = 1 µs
t_d = 10 µs
t_d = 60 µs
520
530
540
λ (nm)
Minimum
Maximum
Normalized intensity
(a)
518,89 nm; Ca I
526,18 nm; Ca I
526,56 nm; Ca I
527,03 nm; Ca I
$B^2\Sigma \rightarrow X^2\Sigma$; CaF
534,95 nm; Ca I
t_d = 10 µs
610 µm height
280 µm height
120 µm height
A
B
C
Atomic signal
Molecular signal
Intensity
515
520
525
530
535
540
545
550
λ (nm)
(b)

Figure 2

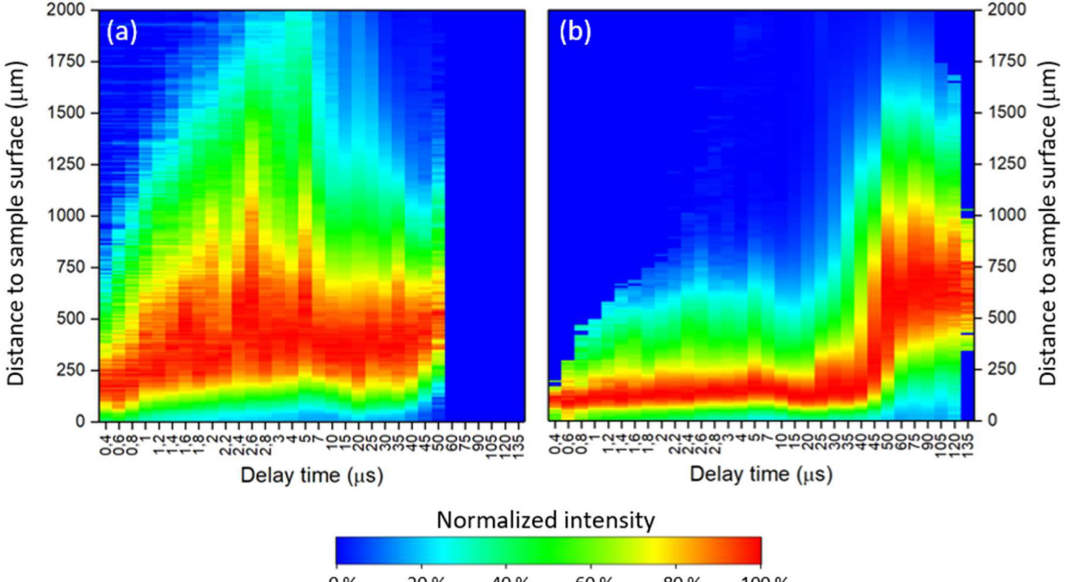
(a)
(b)
Distance to sample surface (µm)
Delay time (µs)
Normalized intensity
0 %
20 %
40 %
60 %
80 %
100 %

Figure 3

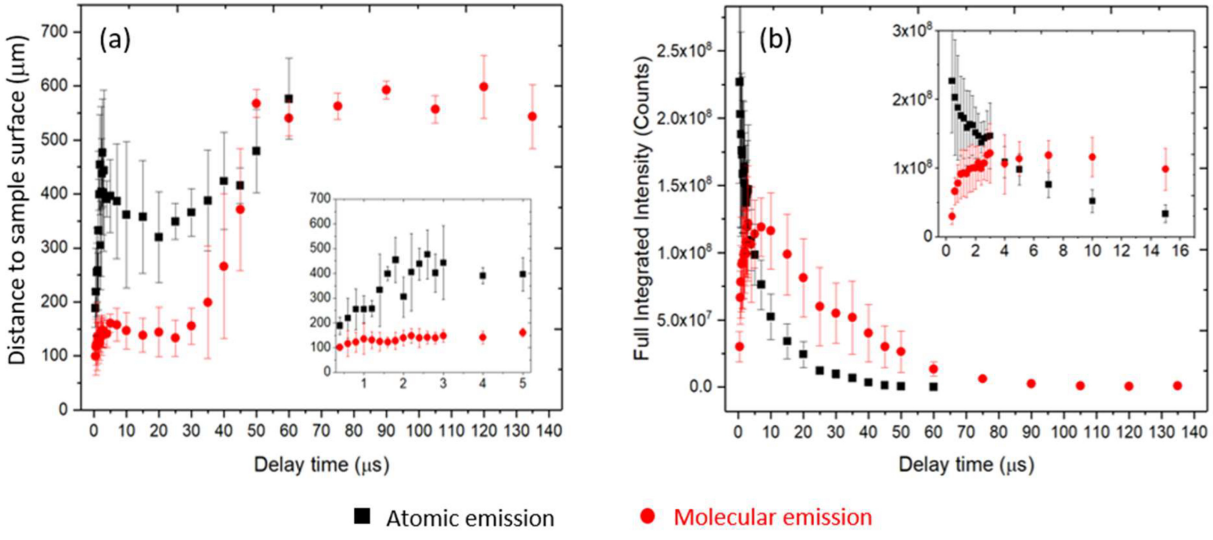
(a)
Distance to sample surface (μm)
Delay time (μs)
(b)
Full Integrated Intensity (Counts)
Delay time (μs)
Atomic emission
Molecular emission

Figure 4

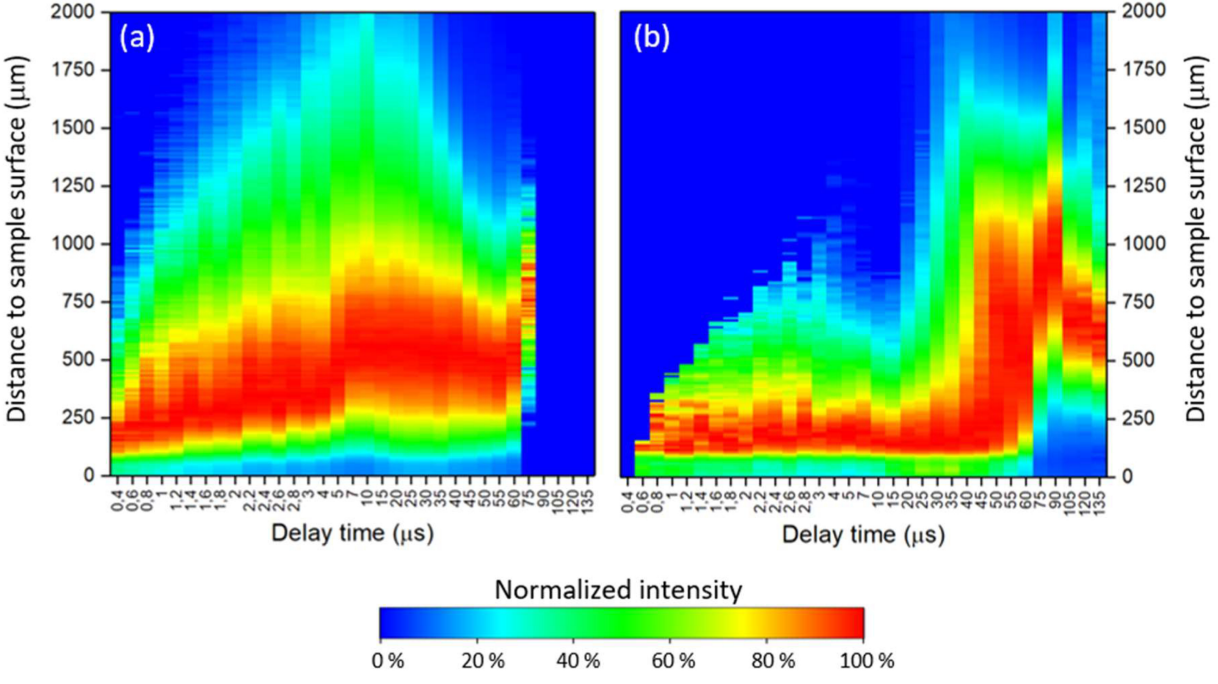
(a)
(b)
Distance to sample surface (µm)
2000
1750
1500
1250
1000
750
500
250
0
0,4 0,6 0,8 1 1,2 1,4 1,6 1,8 2 2,2 2,4 2,6 2,8 3 4 5 7 10 15 20 25 30 35 40 45 50 55 60 75 90 105 120 135
Delay time (µs)
Normalized intensity
0 %
20 %
40 %
60 %
80 %
100 %

Figure 5

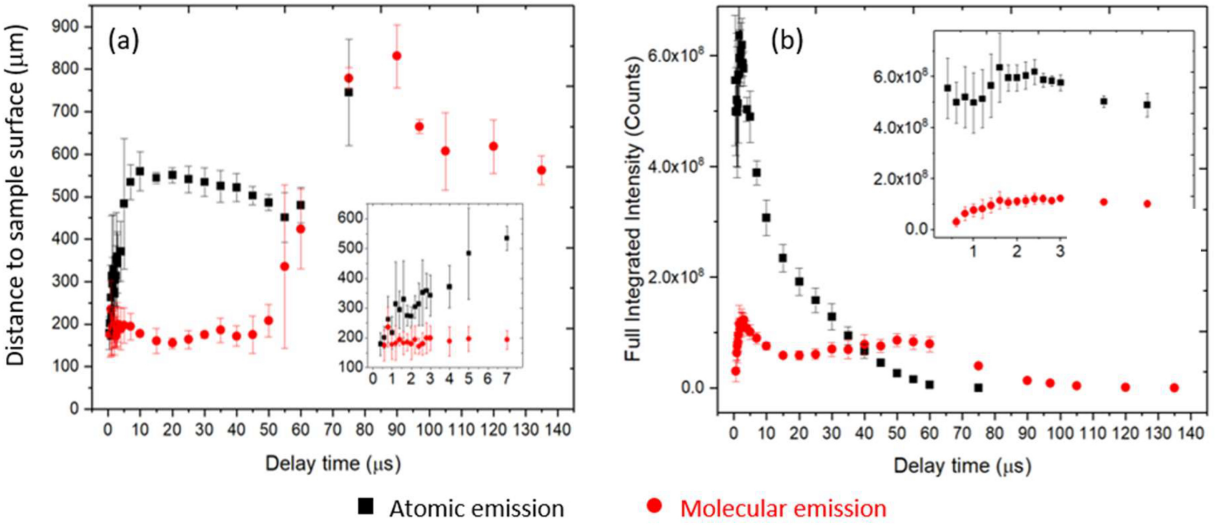
(a)
Distance to sample surface (μm)
Delay time (μs)
(b)
Full Integrated Intensity (Counts)
Delay time (μs)
Atomic emission
Molecular emission

Figure 6